

Convolutional LSTM Neural Networks for Modeling Wildland Fire Dynamics

John Burge^a, Matthew Bonanni^b, Matthias Ihme^{a,b}, Lily Hu^b

^aGoogle Research, Mountain View, CA 94043, USA

^bDepartment of Mechanical Engineering, Stanford University, Stanford, CA 94305, USA

Abstract

As the climate changes, the severity of wildland fires is expected to worsen. Understanding, controlling and mitigating these fires requires building models to accurately capture the fire-propagation dynamics. Supervised machine learning techniques provide a potential approach for developing such models. The objective of this study is to evaluate the feasibility of using the Convolutional Long Short-Term Memory (ConvLSTM) recurrent neural network (RNN) to model the dynamics of wildland fire propagation. The model is trained on simulated wildfire data generated by a cellular automaton percolation model. Four simulated datasets are analyzed, each with increasing degrees of complexity. The simplest dataset includes a constant wind direction as a single confounding factor, whereas the most complex dataset includes dynamic wind, complex terrain, spatially varying moisture content and realistic vegetation density distributions. We examine how effectively the ConvLSTM can capture the fire-spread dynamics over consecutive time steps using classification and regression metrics. It is shown that these ConvLSTMs are capable of capturing local fire transmission events, as well as the overall fire dynamics, such as the rate at which the fire spreads. Finally, we demonstrate that ConvLSTMs outperform non-temporal Convolutional Neural Networks (CNNs), particularly on the most difficult dataset.

Keywords: Recurrent Neural Networks, Convolutional Neural Networks, LSTM, Fire Spread, Percolation Model

Contents

1	Introduction	2
2	Methods: Data Generation	4
2.1	Percolation Model	4
2.2	Datasets	7
2.3	Patch Size	9
3	Methods: Machine Learning	9
3.1	Convolutions on Lattices	9
3.2	Convolutional Neural Networks (CNNs)	9

3.3	Convolutional Long Short-Term Memory (ConvLSTM) Network	12
3.4	Final Dataset Details	15
3.5	Processing Consecutive Predictions and Post Processing	17
3.6	Miscellaneous Training Details	17
4	Results	18
4.1	Performance Metrics	18
4.2	Example: A Single Prediction	20
4.3	Corpus Results	21
4.4	CNN Results	22
4.5	ConvLSTM Results	23
4.6	Unexpected Results	26
5	Conclusions and Future Work	26

1. Introduction

The use of machine learning (ML) in wildfire modeling has seen a significant increase in popularity in recent years, with ML techniques used across tasks such as fuel characterization, risk assessment, fire behavior modeling, and fire management [1]. We focus on fire behavior modeling, specifically forest-scale fire spread modeling. This field has largely favored semi-empirical models, which blend observations from real forest fires and laboratory experiments with physical intuition about the underlying combustion and heat-transfer processes. The most popular among these is that of Rothermel [2], augmented by Albini [3] and Catchpole [4]. These models have been applied both as methods for scientific research and, to a more limited degree, in real-time firefighting efforts [5].

Over recent years, significant progress has been made on the development of models for describing the dynamics of wildfires. These models can be categorized as empirical, semi-empirical, and physical models [6, 7]. Purely empirical models, which rely solely on observations, are not generally favored because they do not translate well across varying environments. Purely physical models, however, are difficult to develop due to the complexity of fire spread behavior, especially given the vast range of fuels, environment, and terrain. Systems with such a great degree of complexity lend themselves naturally to techniques that avoid modeling specific dynamics, perhaps using a high degree of empiricism, or alternatively, ML.

Machine learning has been used to predict fire severity metrics such as the burned area based on field conditions [1, 8]. Kozik et al. [9] simulated fire spread using ML in conjunction with assimilation Geographic Information System data in order to reduce a priori uncertainty. Approaches that use ML alone to explicitly model wildfire dynamics are less common. Hodges and Lattimer [10] used a convolutional neural network (CNN) to predict burn maps on simulated data evolving over six-hour intervals. Their simulated data considered important complexities such as varying canopy height, moisture content, wind and

elevation. Radke et al. [11] used a CNN to predict how a fire front evolves over daily increments, but instead of using simulated data, they applied a CNN model to a single historical fire event.

The dynamics and morphology of the fire front can change significantly over the course of a day, or even over the course of six hours. In a field-fire with homogeneous distribution of fuel, the shape will typically evolve in an orderly fashion. However, for many forest fires with heterogeneous and potentially patchy vegetation distribution, continuously changing wind direction, or variations in terrain, the evolution of the fire-front can become complex and disjoint. Such fires are significantly more difficult to predict [10]. We focus on these fires, as they are more realistic.

Instead of making a single prediction over a relatively large interval, we are concerned with the short-term dynamics on time scales of minutes. To model the spatio-temporal dynamics of the fire front over an extended duration, we use an autoregressive process where one short-term prediction is used to generate the input for a subsequent prediction, and this process is repeated until an approximate six-hour interval is reached. Autoregressive predictions are difficult to make reliably, as errors in the early predictions compound in subsequent predictions. We investigate how well commonly employed CNN models perform at this task. Since fire propagation is an inherently temporal phenomena, we hypothesize that models that explicitly represent temporal relationships are likely to make better predictions. Such models are often referred to as recurrent neural networks (RNNs) [12].

We demonstrate that a particular class of RNNs, the Convolutional Long Short-Term Memory (ConvLSTM) network [13], outperforms CNNs in predicting fire-spread dynamics. ConvLSTM networks combine benefits of using convolutions to model spatially local relationships, like the CNN model does, but add the ability to explicitly model transient dynamics (technically speaking, the ConvLSTM is a type of CNN, but we will use *CNN* to refer to non-temporal CNNs). They have been used broadly in the geosciences, for example, in applications such as the classification of hyperspectral images [14], the evolution of 3D temperature fields in oceans [15], the monitoring of carbon storage reservoirs [16], maritime aerial surveillance [17], and land cover mapping via the combination of multiple satellite datasets [18].

The reference data for the ML model was generated with a semi-empirical model. In contrast to observed wildland fire data, which is often satellite-based, simulated data offers arbitrary temporal and spatial resolution, and allows for the generation of arbitrarily large datasets. Further, the characteristics of the data can be tuned to test the model’s performance in response to specific features.

We present results on four datasets with increasing levels of complexity. The first model is quite simple with only a single source of constant wind as a possible confounding factor, whereas the most complex dataset includes dynamic wind, complex elevation topologies, heterogeneous fuel distributions and spatially varying moisture content.

It is important to acknowledge that, while our data has qualities that represent realistic wildland fire scenarios, the percolation model employed in this work exhibits deficiencies in capturing all relevant physical processes at a quantitative level. Thus, the primary goal of this study is to demonstrate that current RNN models can accurately model the com-

plex relationships that do exist in these semi-empirical wildland fire models. The proposed method is general and applicable to simulated datasets with even more complex dynamics, simulated datasets from physics-based models, or even observational data.

The remainder of this article has the following structure. We start in [Section 2](#) by describing the process used to generate the data. [Section 3](#) introduces the two classes of DNNs we use: the CNN and the ConvLSTM. [Section 4](#) discusses the results, including the performance metrics used on both the ConvLSTM and CNN models across each of the four datasets. In [Section 5](#), we draw conclusions and discuss avenues for future work.

2. Methods: Data Generation

2.1. Percolation Model

The reference data for the ML model was generated with a percolation wildfire spread model based on heat accumulation [19]. This semi-empirical model simulates surface fire spread taking into consideration effects of fuel density, moisture content, slope, and wind. The model is implemented in TENSORFLOW [20], taking advantage of the programming-specific data structures and linear algebra, and enabling the simultaneous calculation of large ensembles.

In the model, the 2D domain with width W and height H is discretized using a lattice with equidistant spacing Δ . This enables the field variables to be represented by matrices of dimension $N_W \times N_H$, where $N_W = W/\Delta$, $N_H = H/\Delta$. At each discrete time step $t + \Delta t$, each lattice cell absorbs heat from its neighbors, and the amount of heat is weighted by the terrain and wind conditions at those neighbors. Denoting the time-dependent heat content of lattice cell (i, j) by $Q_{ij}(t)$, this model can be expressed by the following discrete form:

$$Q_{i,j}(t + \Delta t) = Q_{i,j}(t) + \sum_{k=-N_R}^{N_R} \sum_{l=-N_R}^{N_R} \Omega_{i,j,k,l}(t) K_{k,l}, \quad (1)$$

where N_R represents the discrete number of neighbors that directly influence the local cell (i, j) . The region of influence depends on the size of the cell's neighborhood [19]. $\Omega_{i,j,k,l}(t)$ is the time-dependent heat accumulation rate, and $K_{k,l}$ is a Boolean matrix representing the interacting neighborhood.

[Equation \(1\)](#) is effectively a discrete convolution of the spatio-temporally varying heat-accumulation kernel Ω over the image matrix K . Ω is evaluated taking into consideration the terrain, wind, and ignition state [19]:

$$\Omega_{i,j,k,l} = \Phi_{i,j,k,l} \odot \Psi_{i,j,k,l} \odot L_{i,j}, \quad (2)$$

where \odot denotes the Hadamard (or element-wise) product. The slope factor $\Phi_{i,j,k,l}$, accounting for the local change in terrain, is given as:

$$\Phi_{i,j,k,l} = \exp \left(\alpha_s \frac{(k, l)^T}{\sqrt{k^2 + l^2}} \cdot \vec{S}_{i+k, j+l} \right), \quad (3)$$

where α_s is the slope sensitivity factor, and \vec{S} is the gradient of the terrain altitude Z

$$\vec{S}_{m,n} = \frac{1}{2\Delta} (Z_{m+1,n} - Z_{m-1,n}, Z_{m,n+1} - Z_{m,n-1})^T . \quad (4)$$

The wind factor, $\Psi_{i,j,k,l}$, is modeled to yield an elliptical fire front in a continuous, homogeneous field, as described by Catchpole [4]:

$$\Psi_{i,j,k,l} = 1 + \alpha_w \frac{ab^2\varepsilon \cos(\Theta_{k,l}) + ab\Gamma_{k,l}}{a^2 \sin^2(\Theta_{k,l}) + b^2 \cos^2(\Theta_{k,l})} , \quad (5)$$

with

$$\Gamma_{k,l} = \sqrt{a^2 \sin^2(\Theta_{k,l}) - a^2\varepsilon^2 \sin^2(\Theta_{k,l}) + b^2 \cos^2(\Theta_{k,l})} , \quad (6a)$$

$$\Theta_{k,l} = \cos^{-1} \left(\frac{\vec{U}}{\|\vec{U}\|} \cdot \frac{(k,l)^T}{\sqrt{k^2 + l^2}} \right) , \quad (6b)$$

$$\zeta = 1 + \frac{1}{4} \|\vec{U}\| , \quad (6c)$$

$$\varepsilon = \sqrt{1 - \zeta^{-2}} , \quad (6d)$$

$$a = \frac{\|\vec{U}\| \Delta t}{1 + \varepsilon} , \quad (6e)$$

$$b = \frac{a}{\zeta} , \quad (6f)$$

where $\Theta_{k,l}$ is the angle between the wind direction and the vector towards the lattice cell, α_w is the wind sensitivity factor, ζ is the ellipse length-to-width ratio, ε is the ellipse eccentricity, and a and b are the ellipse semi-minor and semi-major axes, respectively. While this formulation assumes a spatially uniform wind \vec{U} , it can be directly extended to a non-uniform wind $\vec{U}_{i,j}$, where ζ , ε , a , and b also become 2D tensors instead of scalars, and $\Theta_{k,l}$ and $\Gamma_{k,l}$ become 4D tensors $\Theta_{i,j,k,l}$ and $\Gamma_{i,j,k,l}$.

The ignition state tensor, $L_{i,j}$, is activated when sufficient heat has accumulated, and deactivated when the burn duration has been reached. This can be represented by a product of Heaviside functions:

$$L_{i,j}(t) = \mathfrak{H} (Q_{i,j}(t) - Q_{i,j}^{ign}) \mathfrak{H} (D_{i,j} - (t - t_{i,j}^{ign})) , \quad (7)$$

where $t_{i,j}^{ign}$ is the time of ignition and $D_{i,j}$ is the burn duration, which is calculated as:

$$D_{i,j} = D^0 R_{i,j} \quad (8)$$

with D^0 being the nominal burn duration and $R_{i,j}$ is the local fuel density. The ignition time $t_{i,j}^{ign}$ is incremented over time in the unburnt cell until sufficient heat is accumulated for ignition to occur:

$$t_{i,j}^{ign}(t + \Delta t) = t_{i,j}^{ign}(t) + (\Delta t) \mathfrak{H} (Q_{i,j}^{ign} - Q_{i,j}(t)) , \quad (9)$$

where $Q_{i,j}^{ign}$ is a tensor representing the amount of heat required to ignite the lattice cell. Following Rothermel’s formulation [2], this quantity is evaluated as:

$$Q_{i,j}^{ign} = Q_{i,j}^{ign,d} + \alpha_m M_{i,j} , \quad (10)$$

where $Q_{i,j}^{ign,d} = Q^0 R_{i,j}$ is the heat required to ignite the cell once dried, Q^0 is the nominal ignition heat, $R_{i,j}$ is the density, α_m is the moisture sensitivity factor, and $M_{i,j}$ is the moisture content. Note that L and t^{ign} both have a dependency on Q , which is resolved as L is initialized with a given fire state, Q is initialized to Q^{ign} at the affected cell, and Q , L , and t^{ign} are then updated sequentially as described.

The kernel $K_{k,l}$, appearing in Eq. (1), represents the non-local interaction with the surrounding neighborhood and is computed as

$$K_{k,l} = \mathfrak{H} \left(N_R - \sqrt{k^2 + l^2} \right) - \delta_{k0} \delta_{l0} \quad \text{for } k, l \in [-N_R, N_R] \quad (11)$$

where δ_{mn} is the Kronecker delta to exclude self-interaction.

This model has not been calibrated to reproduce real wildfire behavior; rather, it was designed to qualitatively emulate the behavior of fire spread. This simplified model yields data that is useful for the training of ML models; neural networks that can successfully model this data are expected to be able to model calibrated data. To this end, values for the given parameters were selected to target the percolation threshold, yielding fires that exhibit heterogeneous spread behavior without burning out prematurely. The parameter values used for the simulations in this work are presented in Table 1.

Table 1: Percolation model parameters used in this work.

Name	Description	Value
Δ	Lattice spacing	1
N_W	Number of points across field width	110
N_H	Number of points across field height	110
N_R	Neighborhood size	3
D^0	Nominal burn duration	3
Q^0	Nominal ignition heat	3
α_m	Moisture sensitivity	1
α_s	Slope sensitivity	0.7
α_w	Wind sensitivity	2

Representative sample outputs from this simulation are depicted in Fig. 1. These samples are taken from the datasets that are further described in Section 2.2. Sample 1, from the *wind* dataset, featuring uniformly sparse, heterogeneous vegetation, no moisture, flat terrain, and wind, demonstrates the response of the fire front to the wind, advancing with a bias towards the south. Sample 2, from the *wind-slope* dataset, is similar to sample 1, except it additionally features a planar, sloped terrain. Despite the forcing from the wind blowing towards the northwest, the fire front responds to the significant slope and burns

uphill to the south-southeast. Finally, sample 3, from the *realistic* dataset, features patchy, heterogeneous vegetation, heterogeneous moisture content, realistic procedurally-generated terrain, and wind. The fire begins in a low valley, and responds to the wind by advancing with a westward bias. Eventually, it reaches regions of steep slope in the south and east of the domain, and burns rapidly up these slopes.

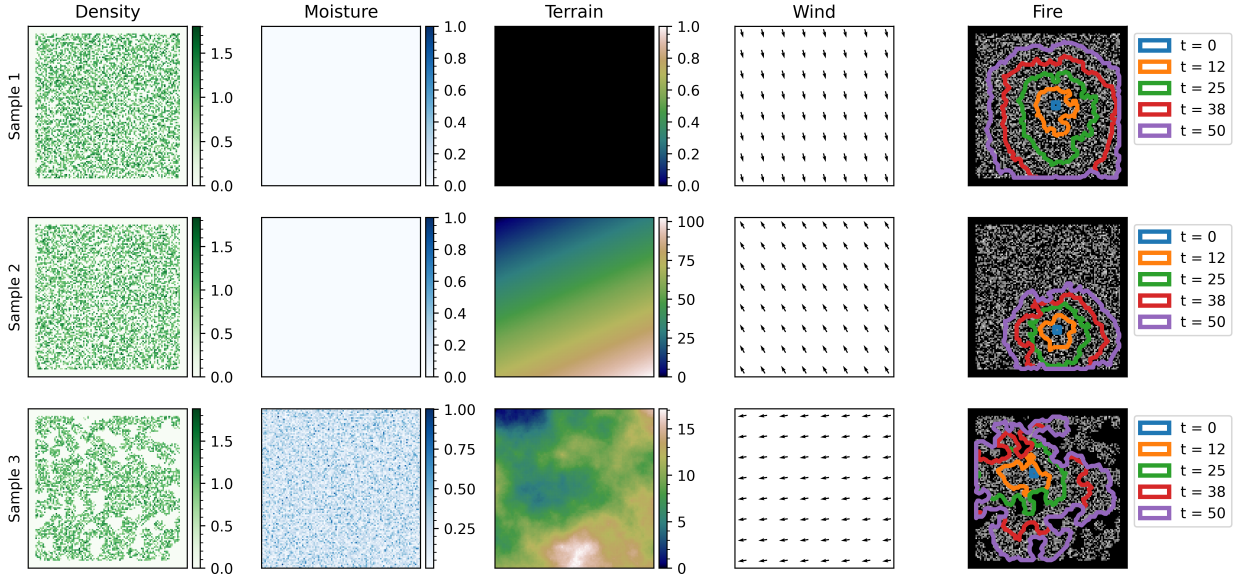


Figure 1: Representative sample input fields and fire spread output of the percolation model. Sample 1 is selected from the *wind* dataset, sample 2 is from the *wind-slope* dataset, and sample 3 is from the *realistic* dataset; see Table 2 for details on the datasets.

The model also responds to temporally varying wind, as depicted in Fig. 2. This simulation exercises all of the features of the percolation model. The flame front has a complex shape due to the heterogeneity of the fuel and terrain. At time step $t = 20$, it can be seen that the front has responded to the eastward wind. At $t = 40$, the wind has changed direction and the fire has responded by advancing in the southwest direction. We also note that it has continued to burn to the northeast despite the adverse wind, because of the favorably sloped terrain.

2.2. Datasets

The percolation model described in Section 2.1 was used to generate data to train the ML models. A total of four data sets were generated, each containing 1000 independent fire sequences. In each sequence, the environmental conditions of the field were randomly varied, with different datasets exhibiting different characteristics. The dataset characteristics are summarized in Table 2.

In the first three datasets, 50% of the cells (uniformly sampled) were filled with fuel of randomly assigned, normally distributed density ($\mu = 1, \sigma = 0.25$) These cases assumed no moisture content. The *wind* dataset was designed to test the model performance with

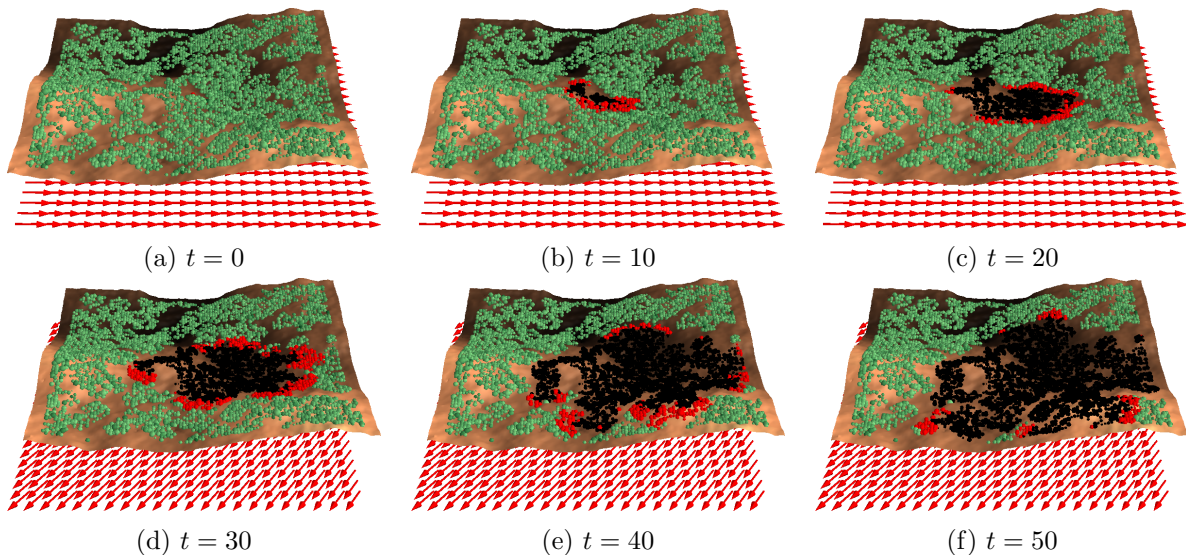


Figure 2: Visualization of a representative sample output from the *realistic* dataset at successive time steps. The ground color corresponds to terrain altitude, and the arrows depict spatially constant but temporally changing wind direction.

Table 2: Distinguishing characteristics of data sets used for training ML models.

ID	Fuel Placement	Density	Moisture	Terrain	Wind
<i>wind</i>	Uniformly sparse	Heterogeneous	None	Flat	Constant
<i>wind-slope</i>	Uniformly sparse	Heterogeneous	None	Planar	Constant
<i>dynamic wind</i>	Uniformly sparse	Heterogeneous	None	Flat	Variable
<i>realistic</i>	Patchy	Heterogeneous	Heterogeneous	Realistic	Variable

a single confounding factor: a wind blowing in a constant direction for the entire duration of the fire and across the entire forest patch. The two vector components of the wind were generated with uniform distributions in the range $[-7, 7]$. The *wind-slope* dataset was designed to test model performance with multiple, potentially competing confounding factors by adding a planar slope to the terrain. Each of the 1000 fire sequences was given both a random wind (generated in the same manner as before) and a terrain with a slope of random grade (uniform distribution, $\theta \in [0, \pi/4]$) and azimuth (uniform distribution, $\phi \in [0, 2\pi]$). The *dynamic wind* dataset was designed to test the response of the model to time-varying input and featured wind (uniform distribution, components $\vec{U} \in [-12, 12]$) which changed in both speed and direction after exactly 30 time steps. Fuel was arranged randomly as in the first two datasets. The final dataset is the *realistic* dataset and includes all complexity available in the model described in Section 2.1. It featured patchy fuel placement which is representative of real forests (though vegetation growth patterns are not correlated with terrain as would be expected in a real forest). This vegetation was generated by placing circular areas of vegetation of radius 8 until the field was 70% filled. These areas were then masked, randomly clearing 40% of the cells, and a random density was

assigned to the filled cells (normal distribution, $\mu = 1, \sigma = 0.25$). It also featured random moisture content (folded normal distribution, $\mu = 0, \sigma = 0.25$) and realistic terrain elevation generated using the diamond-square algorithm [21] with a maximum height of 50. Finally, it also featured a dynamic wind change like that of the *dynamic wind* dataset (uniform distribution, components $\vec{U} \in [-12, 12]$).

The burnout time for a single fire is generally between 75 and 200 time steps. Since the data being modeled is simulated, the length of a single time step is not exactly specified, but approximately corresponds to dynamics that occur on the scale of five to ten minutes. Each cell in a simulated field corresponds to roughly the breadth of an average tree, e.g., 10-20 meters. For each case, a spot fire of prescribed size was initiated at a random, uniformly distributed location within the middle 50% of the field.

2.3. Patch Size

We initially used lattices of size (100, 100) cells to represent a patch of forest. The size of the domain was found to be large enough to allow for interesting fire front dynamics to play out, while still being small enough to allow a sufficient number of patches to be stored in memory simultaneously. This is important as the training process for Deep Neural Networks (DNNs) is typically done in batches, so many patches need to be stored in memory at the same time. The optimal size of batches (and thus the number of patches that need to be stored) in DNN training is still an active area of research, but in general, batches that are too small can cause instability issues and pose problems for data normalizing. Batches that are too large simply do not fit into memory. We chose batch sizes of 64. Further details on the batch training can be found in Goodfellow et al. [22].

As all of our models ultimately require a convolutional kernel to be passed across the patch, so we zero-pad the (100, 100) patch with 5 cells around the border. This ensures that every location in the lattice will at some point fall within a location of the convolution kernel. Thus, the final shape of the patches generated is (110, 110).

3. Methods: Machine Learning

3.1. Convolutions on Lattices

We refer to the input of our models, or the input to various layers in the model, as lattices (other common terms include grids, images, or tensors). All of our models apply convolutions to these lattices. For example, the patches of vegetation described in Section 2.3 are lattices showing the location of trees in a field of vegetation. Not all of the lattices processed throughout the various stages of the model correspond to fields. Some correspond to, for example, elevation data or wind velocities. We assume the reader has knowledge of applying convolutions to lattices, which were introduced in Section 2.1. The interested reader is referred to Ref. [22] for additional details.

3.2. Convolutional Neural Networks (CNNs)

A large number of CNNs used in practice follow a common pattern popularized by the autoencoder [23]. An autoencoder is a DNN that is broken up into two main sections: the

encoder and the decoder, Fig. 3a. The encoder attempts to reduce the lattice into a set of parameters that describe the variance seen in the input. The last layer in the encoder is often called the bottleneck, and is treated as input to the next stage: the decoder. The decoder takes the features in the bottleneck and regenerates the original lattice.

Instead of regenerating the input lattice, it is also possible to use the same network structure to generate a new lattice. In our case, that new lattice will be the location of the fire front in the next time step of the simulation. Thus, our CNN is a so-called autoencoder-like network. That is, it has the same structure as an autoencoder, but the predictive task is different. We use the autoencoder as a baseline that roughly corresponds to the work of Hodges and Lattimer [10]. We could not use their exact model, as the bottleneck of their model employed a fully-connected layer with millions of parameters that cannot scale much beyond the (50, 50) patches they used.

The structure of our autoencoder-like model is shown in Fig. 3a. It starts off with the input lattices of shape (N_H, N_W, N_c) with N_c being the number of channels. Both N_H and N_W are set to 110. N_c varies based on the particular dataset used, but ranges between five and seven.

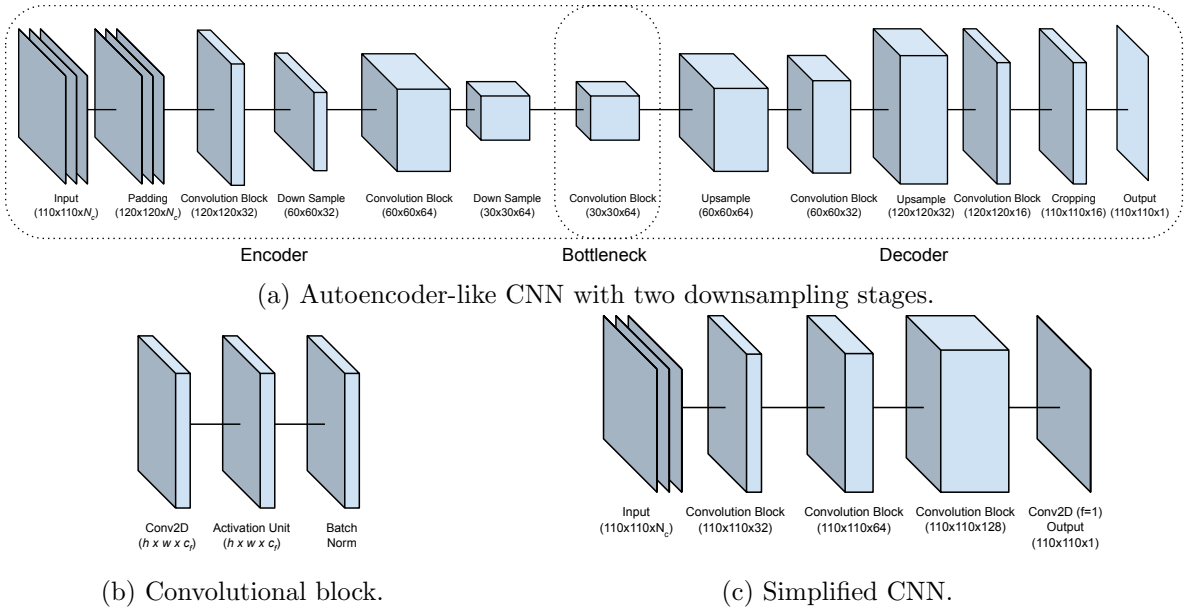


Figure 3: CNN architectures employed in the present work. (a) Autoencoder-like CNN with two downsampling stages. (b) Convolutional block. c_f is the number of filters applied in the convolution. (c) Simplified CNN.

Since the model will repeatedly downsample the input, it is important that a down-sample is never applied to an odd-sized height or width, as that would introduce aliasing during upsampling. Since our patches have patch dimensions of 110, the first stage in the model zero-pads the patch to be (120, 120, *channels*). This value was chosen, as it can be downsampled twice, which is the limit of downsampling we investigated.

The model then repeatedly applies a convolutional block, Fig. 3b, and then a downsam-

pling block. That is repeated twice, resulting in a bottleneck lattice with spatial dimensions of (30, 30). The decoder takes that lattice, repeatedly applies an upsample operation (interpolating newly added values via a nearest neighbors algorithm) and another convolutional block. The network is terminated via a single 2D convolution with a single filter, resulting in an output shape of (110, 110, 1).

We also investigate a simplified version of this CNN where we remove the downsampling operations, which results in the much simpler overall structure as shown in Fig. 3c.

All DNNs will ultimately have a set of hyperparameters that impact the structure, parameters and training efficacy of the model. Indeed, one of the main difficulties in training DNNs is the need to empirically identify the best settings to these hyperparameters. The following are the most important hyperparameters in our model:

- $\text{lr} \in \{10^{-2}, 10^{-3}, 10^{-4}, 10^{-5}, 10^{-6}\}$ indicates the learning rate. This influences how quickly the training process iteratively makes updates to the model. Values that are too small result in unnecessarily long training times and values that are too large prevent good solutions from being identified.
- $\text{ks} = \{3, 5\}$ specifies the kernel size for both the height and width dimensions of the convolutions. We briefly experimented with $\text{ks} = 3$, but it quickly became apparent models using $\text{ks} = 5$ performed much better.
- $\text{au} \in \{\text{ReLU}, \text{LeakyReLU}\}$ specifies which activation unit to use after convolutional blocks. There are many more possibilities, but these are two of the most commonly used and we did not feel the need to investigate alternatives.
- $\text{ds} \in \{\text{yes}, \text{no}\}$ indicates whether to include downsampling stages: **yes** indicates that the structure shown in Fig. 3a should be used and **no** indicates the structure shown in Fig. 3c should be used.
- $\text{bn} \in \{\text{yes}, \text{no}\}$ indicates whether batch normalization stages are included in the convolutional block.
- $\text{cb} \in \{1, 2, 3\}$ specifies the number of convolutional blocks (and downsampling stages, if enabled) that are included.
- nf is a list of length cb specifying the number of filters in each of the convolutional blocks. For example, $\text{nf} = [16, 32, 64]$ indicates that the three convolutional blocks in the encoder would contain 16 filters, then 32 filters and finally 64 filters, whereas the convolution blocks in the decoder would contain 64 filters, then 32 filters, then 16 filters.
- $\text{bf} \in \{8, 16, 32, 64, 128, 256\}$ specifies the number of filters in the bottleneck. We always set this to the number of filters in the last convolutional block.

It is not possible to exhaustively train on all possible combinations of these hyperparameters, however, we searched through many combinations of these parameters to empirically

find the best settings for each hyperparameter. For example, we found that downsampling always returned worse results than a model with all other hyperparameters set to the same value. Thus, we concluded that downsampling was not helpful. Similarly, we empirically determined that batch normalization was detrimental to model performance, and that the better activation unit to use was ReLU as opposed to LeakyReLU. The learning rate was chosen early on as the rate that appeared to allow training to proceed at a reasonable rate, and kept the same across all subsequent training.

Ideally, we would perform a hyperparameter search independently for each dataset, however, this is not feasible. So, to reduce the amount of training required, we performed the hyperparameter search on the *realistic* dataset, and then used those same hyperparameters across all datasets. It is possible that separate hyperparameter searches for each dataset would result in stronger models.

When comparing two competing sets of hyperparameters, we would ideally let the two models train completely through to convergence, i.e., the point at which additional training rounds (or epochs) bring no further improvements to the loss function. The loss function is the specific function that is being optimized during training. Here, the loss function is the mean squared error between the cells in the predicted lattice and the cells in the training label. Training a single model to convergence typically takes multiple days and could require up to 400 epochs of training.

To speed up the hyperparameter search process, if two competing models showed a difference in their loss functions that was approximately an order of magnitude, the loss function would be used as a proxy for performing a full evaluation when using a more robust set of performance metrics. For example, when testing the `ds` hyperparameter, we noted after 200 epochs that every model being trained with downsampling had a loss function that was approximately 10^{-5} , whereas all comparative models that didn't downsample had loss functions of around 10^{-6} . We never observed a model with that much higher loss perform better on our final evaluation, so using the loss function as a proxy for the full evaluation seems reasonable. However, we observed that smaller differences in loss functions did not always correspond to the same ranking on the full evaluation and always let those models train fully through convergence. Our final settings for these hyperparameters are:

$$\{\text{ds} = \text{no}, \text{bn} = \text{no}, \text{cb} = 3, \text{nf} = [32, 64, 128], \text{bf} = 128, \text{ks} = 5, \text{au} = \text{ReLU}\}.$$

In all, we trained approximately 30 different models to identify this representative case.

3.3. Convolutional Long Short-Term Memory (ConvLSTM) Network

The main weakness of the CNN approach is the lack of explicitly modeling the transient dynamics in the wildfire data. One of the most common deep learning methods for modeling such relationships is to employ a RNN [12] and in particular the LSTM [24]. All RNNs attempt to track some evolving state over time, and the LSTM is considered one of the dominant methods due to the introduction of its memory cell, c , which can accumulate and forget states being tracked from time-step to time-step. This innovation allows the LSTM to alleviate one of the main disadvantages of other RNNs: forgetting some state before

that state becomes useful. The memory cell in the LSTM allows the model to explicitly determine which state will be helpful to remember, and which state can safely be forgotten. LSTMs also provide protection against the issue of vanishing gradients, i.e., gradients of the loss function that turn into zeros as they propagate backwards through the network during training.

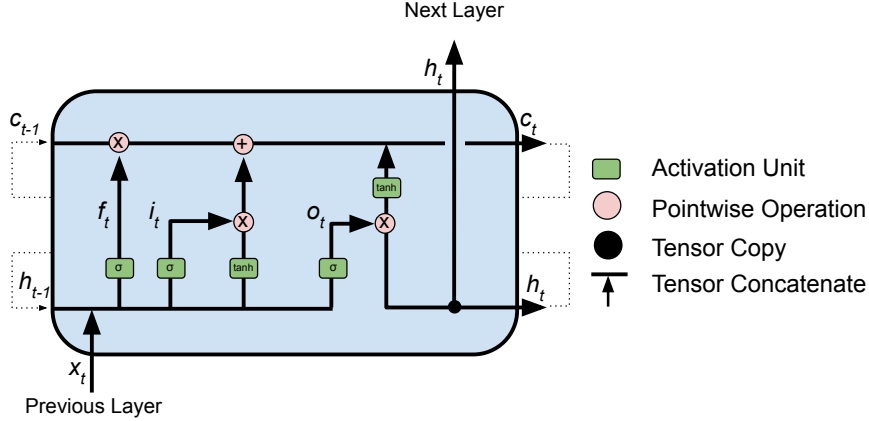


Figure 4: Structure of a single LSTM block. Stacked LSTM blocks connect the h_t output of the first block, with the x_t input of the next block. The C_t and h_t outputs on the right, feed into their corresponding inputs on the left for each time step provided. The dotted line indicates crossing time steps.

The core layer of an LSTM model is the LSTM block, shown in Fig. 4. The output of an LSTM block, h , is composed of multiple time steps, $h_t, 0 \leq t < T$ where T corresponds to the number of time steps in the input training instances. We fixed T to 10, though other similar values would likely be reasonable. For each time step in the input, h_t is computed via the following set of update equations:

$$i_t = \sigma(W_{xi}x_t + W_{hi}h_{t-1} + W_{ci} \odot c_{t-1} + b_i) , \quad (12a)$$

$$f_t = \sigma(W_{xf}x_t + W_{hf}h_{t-1} + W_{cf} \odot c_{t-1} + b_f) , \quad (12b)$$

$$c_t = f_t \odot c_{t-1} + i_t \odot \tanh(W_{xc}x_t + W_{hc}h_{t-1} + b_c) , \quad (12c)$$

$$o_t = \sigma(W_{xo}x_t + W_{ho}h_{t-1} + W_{co} \odot c_t + b_o) , \quad (12d)$$

$$h_t = o_t \odot \tanh(c_t) , \quad (12e)$$

where x_t is the input at time t , the various W matrices and b vectors are weights learned during model training and σ is the sigmoid function. Further details on the LSTM model formulation can be found in Shi et al. [24].

While successful in many domains, the LSTM is a poor choice for modeling lattice data, due to the large number of weights and large matrix multiplications required to parameterize every cell in the lattice. We overcome this by utilizing Convolutional LSTMs [13], in which the large matrix multiplications are replaced with convolutions, drastically reducing the number of parameters needed to train, while still parameterizing the relationships among

neighboring cells in the input. This replaces the update equations in Eq. (12) with:

$$\mathcal{I}_t = \sigma(W_{xi} * \mathcal{X}_t + W_{hi} * \mathcal{H}_{t-1} + W_{ci} \odot \mathcal{C}_{t-1} + b_i) \quad (13a)$$

$$\mathcal{F}_t = \sigma(W_{xf} * \mathcal{X}_t + W_{hf} * \mathcal{H}_{t-1} + W_{cf} \odot \mathcal{C}_{t-1} + b_f) \quad (13b)$$

$$\mathcal{C}_t = f_t \odot \mathcal{C}_{t-1} + \mathcal{I}_t \odot \tanh(W_{xc} * \mathcal{X}_t + W_{hc} * \mathcal{H}_{t-1} + b_c) \quad (13c)$$

$$\mathcal{O}_t = \sigma(W_{xo} * \mathcal{X}_t + W_{ho} * \mathcal{H}_{t-1} + W_{co} \odot \mathcal{C}_t + b_o) \quad (13d)$$

$$\mathcal{H}_t = \mathcal{O}_t \odot \tanh(\mathcal{C}_t) \quad (13e)$$

where \mathcal{H}_t is the output at time t , \mathcal{X}_t , is the input at time t and $*$ is the convolution operation. The initial input to an ConvLSTM block, \mathcal{X} , is a tensor of shape (T, N_H, N_W, N_c) , where T is the number of time steps. In the first ConvLSTM block, N_c is the number of channels in the input data, and for subsequent blocks, N_c is the number of filters in the convolutions of the previous ConvLSTM block. \mathcal{X}_t refers to the input at the t^{th} time step, and thus, has a shape of (N_H, N_W, N_c) .

The output of the ConvLSTM block shares the same shape as the input, except the number of channels is set to the number of filters in the convolutions. The lattice being output by that block is the result of those filters being applied to the input of that block. Thus, subsequent ConvLSTM blocks apply convolutions to output of previous convolutions, which allows each subsequent ConvLSTM block to identify more complex and abstract relationships in the data than the previous block. The structure of the ConvLSTM model is illustrated in Fig. 5.

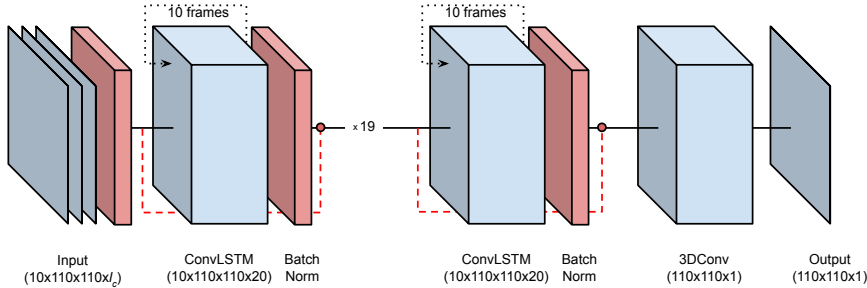


Figure 5: Structure of the ConvLSTM model. The black dotted line on the ConvLSTM blocks indicate the number of frames processed internally in the block, where N_c indicates the number of channels in the input. The red dotted line corresponds to a skip link, which is implemented as a Conv3D layer with kernel size $(1, 1, 1)$. Both the skip link and the batch normalization blocks are highlighted in red to indicate that they were not actually included in our best performing model. We visualize them here, as these are common additions to ConvLSTMs that should be empirically evaluated.

Similar to CNNs, finding the optimal structure for LSTMs requires an empirical hyperparameter search. The settings for the learning rate, kernel size, and activation unit were kept the same as they were in the CNN. Keeping those same values did not appear problematic, though additional empirical experiments could potentially find better values. We performed an empirical search on the following hyperparameters:

- $\text{nb} \in (0, 10]$ specifies the number of stacked blocks.

- $\text{fpb} \in (0, 20]$ specifies the number of filters to use per ConvLSTM block.
- $\text{bn} \in \{\text{yes}, \text{no}\}$ specifies whether batch normalization was used after each ConvLSTM block.
- $\text{do} \in \{0.0, 0.01, 0.05\}$ specifies how much dropout to use in the convolutional layers (i.e., what fraction of network nodes should be randomly reset to 0.0 after each epoch).
- $\text{s1} \in \{\text{yes}, \text{no}\}$ specifies whether skip links are added for each of the stacked blocks.

In general, we found that increasing either fpb or nb resulted in model quality increasing. Ultimately, after iteratively increasing these values to $\text{fpb} = 20$ and $\text{nb} = 10$, the memory on the NVIDIA P100 GPUs was maxed out and further increases were not feasible. Additional complexity likely would help to some degree, but clear signs of diminishing returns were observed by this point. Batch normalization, drop out and skip links were all found to be unhelpful across multiple configurations. So the final representative ConvLSTM model had the hyperparameter settings:

$$\{\text{nb} = 10, \text{fpb} = 20, \text{bn} = \text{no}, \text{do} = 0.0, \text{s1} = \text{no}\}.$$

In particular, it was surprising to see that skip links weren't helpful, as they often help training models with many consecutive stages [25], though as mentioned above, LSTM models are inherently resistant to issues like vanishing gradients, potentially lowering the utility of adding residual links.

3.4. Final Dataset Details

The four datasets (see Table 2) are set up slightly differently for the CNN models versus the ConvLSTM model. Sections 3.2 and 3.3 provide a detailed discussion of these models, but with respect to their input data, the main difference is that the CNN model requires a single time point in a fire sequence as input, and the ConvLSTM requires a sequence of consecutive time points in a fire sequence as input. For the CNN, a single batch of data has the shape (N_b, N_H, N_W, N_c) , where $N_b = 64$ is the batch size, $N_H = N_W = 110$, and N_c indicates the number of channels in the lattice. For the ConvLSTM, a single batch of data has the shape $(N_b, N_t, N_H, N_W, N_c)$, where $N_t = 10$ is the number of sequential frames placed in a single training instance (note that $N_t \ll N_\tau$, the total number of lattices generated in a single fire sequence).

All four data sets have the same initial 3 channels. The first channel is the *vegetation channel* and contains the location of all vegetation mass that has not yet burned. The second channel is the *firefront channel* and contains the location of the fire-front in the previous time-step. The third channel is the *ash channel* and contains the location of all vegetation that has burnt so far. Thus, at any time in the sequence, the *vegetation channel* plus the *ash channel* is constant and equal to the starting configuration of vegetation before the fire started.

Both the *firefront channel* and the *ash channel* do not actually provide the model more data than it already has, since these two frames can ultimately be derived from the current

vegetation channel and the *vegetation channel* from the previous time step. However, we found early on that explicitly adding these channels made predictions significantly better for the models.

All four data sets have wind velocity added as the fourth and fifth channel, where the fourth channel indicates the wind’s horizontal intensity, and the fifth channel specifies the wind’s vertical intensity. Since wind is spatially constant, these channels are filled in with constant values. In the *dynamic wind* and *realistic* dataset, these constant values change at time step 30 to a new randomly sampled direction.

The *wind-slope* and *realistic* dataset have the terrain height specified as the sixth channel. Finally, the *realistic* dataset has the moisture content for each patch of vegetation added as its seventh channel.

All channels were manually normalized prior to training (as opposed to batch normalization). The *wind channels* are the only channels that include negative values, and thus were normalized to have unit variance and zero mean. All other channels were normalized to range between 0.0 and 1.0 based on the min and max values seen throughout a single dataset. Normalization is not done across data sets.

The sequence for an individual fire is broken up into as many disjoint sequences of 10 time steps as possible. For example, a sequence of 75 time steps will result in seven training instances. An example of a single frame of data for the *realistic* data set is shown in Fig. 6.

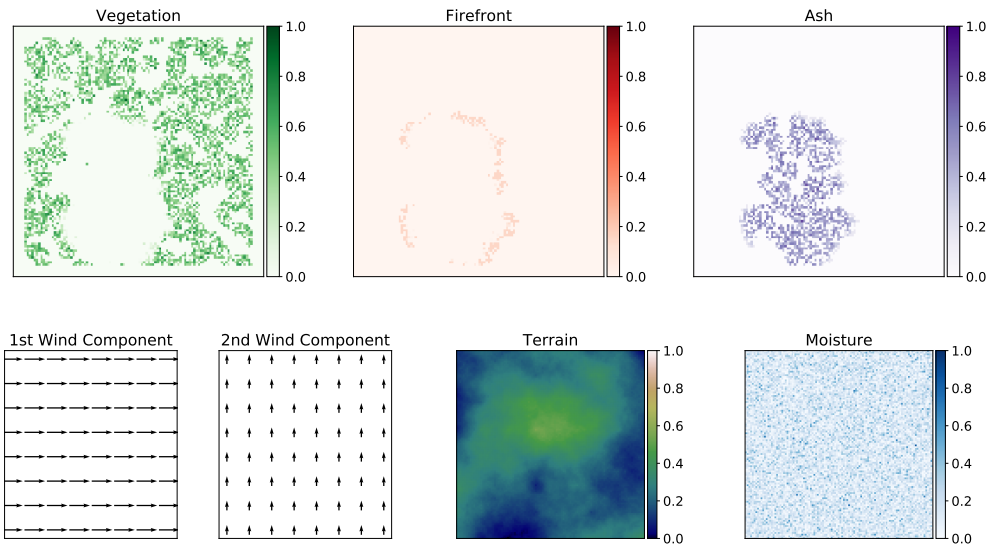


Figure 6: An example of the seven input channels for a single training instance in the *Realistic* dataset

The first 10 time steps of a fire sequence are discarded in the CNN, so the CNN can start making predictions at the same time step that the ConvLSTM model does (recall that the ConvLSTM needs those first 10 time steps as its single initial training instance). The label for all predictions is exactly the same. It is the location that the fire front will transition to, in this time step.

3.5. Processing Consecutive Predictions and Post Processing

To measure how well our models estimate the dynamics of wildfire propagation, a model’s predictive efficacy cannot just be measured on making one single prediction. Instead, the performance of the model making many consecutive predictions is measured. To facilitate this, we start with input data as defined in Section 3.4. Given a trained model, we get the predicted value for that training instance. We use that prediction to update the training instance for the next consecutive prediction via Algorithm 1.

Algorithm 1 Autoregressive process for generating consecutive predictions.

```
datapoint0 ← the initial training instance described in Section 3.4.  
prediction0 ← the prediction for datapoint0.  
for i in range(1:50) do  
  datapointi ← datapointi-1.  
  Subtract predictioni-1 from the vegetation channel in datapointi.  
  Replace any negative values in the new vegetation channel with 0.0  
  Add predictioni-1 to the ash channel in datapointi.  
  Set the firefront channel in datapointi to be equal to predictioni-1.  
  Set wind channels in datapointi to be equal to the wind at time step i.  
  Remove the first time step from datapointi (so it stays length 10).  
  predictioni ← the prediction for datapointi  
end for
```

Preparing the consecutive input for the CNN is basically the same, except the training instances for the CNN only contain a single time point, so that the i^{th} training instance doesn’t contain any of the frames from the previous data instances. An additional post-processing step was necessary for the CNN, as the CNN would occasionally accumulate very small errors over consecutive predictions that would eventually cause fires to ignite in a random location on the domain. This was resolved by simply setting any predicted value less than 0.025 to zero. Virtually all actual burn values are above 0.025, but there are a small number of burn states that legitimately fall in this range. Adding hard physical constraints to DNNs is an active area of research, and had this simple post-processing step been insufficient, a more elegant solution for enforcing this constraint in the model could have been investigated, for example, see [26]. Note that the LSTM did not need this post-processing step as it was more effective at controlling the buildup of these small errors than the CNN.

3.6. Miscellaneous Training Details

Each of the 1000 fire sequences in each of the four datasets are partitioned into 200 sequences for the testing dataset and 800 sequences for the training dataset. An additional 200 fire sequences were made for the *realistic* dataset, and were used as validation dataset for hyperparameter training.

All models were built in TENSORFLOW 2.0 [20], with EAGER MODE enabled. Keras APIs [27] were used to build the model and the datasets. We trained our models on a single

machine with 16 CPU cores and eight NVIDIA P100 GPUs—a configuration readily available on most modern cloud ML platforms. Keras’s distributed strategy, `MIRROREDSTRATEGY` was used to coordinate multi-GPU training. The ADAM optimizer [28] was used. Training was allowed to proceed for 400 epochs, at which point all loss functions appear to have converged, though we acknowledge that detecting convergence is non trivial. It is possible that additional training epochs could potentially improve any of the models we trained. No noise was added to the input data. The loss function used was mean squared error, specifically, the Keras loss function `tf.keras.losses.MeanSquaredError`.

4. Results

Our ML models predict the spatio-temporal evolution of the fire front over a succession of 50 time steps, spanning approximately an hour of physical time. This section describes how accurately the CNNs and the ConvLSTM perform on that regression.

4.1. Performance Metrics

For each cell in an input lattice, each of the models returns a floating point value indicating how much vegetation in that cell will burn away at that point in time. One of the most obvious ways to measure how well the regression is performing is to compute the mean squared error, MSE , between the label and the predicted value. Given an input, \mathcal{X} , its corresponding label, \mathcal{Y} , and the prediction $\hat{\mathcal{Y}}$:

$$MSE(\mathcal{Y}, \hat{\mathcal{Y}}) = \frac{1}{N_H N_W} \sum_{i=1}^{N_H} \sum_{j=1}^{N_W} |\hat{\mathcal{Y}}_{ij} - \mathcal{Y}_{ij}|^2. \quad (14)$$

Note that the MSE metric is quite demanding (and is used as our loss function during training). For example, a model might do a good job predicting the general shape of the fire front, but might make errors in how quickly that front spreads. The MSE could penalize this model just as much as a model that predicted the fire went in the completely opposite direction. Small errors in estimating the speed of the fire can also result in large MSE . Given that predicting the speed of the fire is often of utmost importance, we also measure the error of the total amount of fire at each point in time, the summed total error, STE :

$$STE(\mathcal{Y}, \hat{\mathcal{Y}}) = \left| \sum_{i=1}^{N_H} \sum_{j=1}^{N_W} \hat{\mathcal{Y}}_{ij} - \sum_{i=1}^{N_H} \sum_{j=1}^{N_W} \mathcal{Y}_{ij} \right|. \quad (15)$$

Of course, STE is also not a perfect indicator of the quality of the prediction. It could report a low error for a fire that was burning at the correct rate, but in the completely opposite direction. So, models that have low STE are predicting the correct rate of fire, and models that have low MSE are predicting the correct location of the fire.

In addition to tracking regression statistics, we also track classification statistics by converting the regressed value into a binary classification. This is done by introducing a threshold, below which a cell is said to be not on fire and above which a cell is said to be

on fire. We use a threshold of 0.1, which captures the majority of cells legitimately on fire, though does obfuscate some actual fires of the smaller patches of vegetation in a sample. Binary classification performance is typically measured by the terms of the confusion matrix [29]: True Positives (TP), True Negatives (TN), False Positives (FP) and False Negatives (FN). In the following, we summarize the functional relations of these terms: Let I^θ be an indicator variable that is 1 when $\theta \geq 0.1$ and let $\overline{I^\theta}$ be its complement. We can compute the total number of positive and negative classifications in the ground truth:

$$P(\mathcal{Y}) = \sum_{i=1}^{N_H} \sum_{j=1}^{N_W} I^{\mathcal{Y}_{ij}} , \quad (16a)$$

$$N(\mathcal{Y}) = \sum_{i=1}^{N_H} \sum_{j=1}^{N_W} \overline{I^{\mathcal{Y}_{ij}}} . \quad (16b)$$

To compute the terms of the confusion matrix, we use the following indicator functions:

$$I^{TP_{ij}} = I^{\mathcal{Y}_{ij}} \wedge I^{\widehat{\mathcal{Y}}_{ij}} , \quad I^{TN_{ij}} = \overline{I^{\mathcal{Y}_{ij}}} \wedge \overline{I^{\widehat{\mathcal{Y}}_{ij}}} , \quad I^{FP_{ij}} = \overline{I^{\mathcal{Y}_{ij}}} \wedge I^{\widehat{\mathcal{Y}}_{ij}} , \quad I^{FN_{ij}} = I^{\mathcal{Y}_{ij}} \wedge \overline{I^{\widehat{\mathcal{Y}}_{ij}}} . \quad (17)$$

The terms of the confusion matrix are thus:

$$TP(\mathcal{Y}, \widehat{\mathcal{Y}}) = \sum_{i=1}^{N_H} \sum_{j=1}^{N_W} I^{TP_{ij}} , \quad (18a)$$

$$TN(\mathcal{Y}, \widehat{\mathcal{Y}}) = \sum_{i=1}^{N_H} \sum_{j=1}^{N_W} I^{TN_{ij}} , \quad (18b)$$

$$FP(\mathcal{Y}, \widehat{\mathcal{Y}}) = \sum_{i=1}^{N_H} \sum_{j=1}^{N_W} I^{FP_{ij}} , \quad (18c)$$

$$FN(\mathcal{Y}, \widehat{\mathcal{Y}}) = \sum_{i=1}^{N_H} \sum_{j=1}^{N_W} I^{FN_{ij}} , \quad (18d)$$

In addition, we introduce Recall (Rc) (the fraction of positives that were predicted to be positives) and Precision (Pr) (the fraction of positive predictions that were positives) which are used to compute the F1-score ($F1$) (the harmonic mean of precision and recall) as our primary metric.

$$Pr(\mathcal{Y}, \widehat{\mathcal{Y}}) = \frac{TP(\mathcal{Y}, \widehat{\mathcal{Y}})}{TP(\mathcal{Y}, \widehat{\mathcal{Y}}) + FP(\mathcal{Y}, \widehat{\mathcal{Y}})} , \quad (19a)$$

$$Rc(\mathcal{Y}, \widehat{\mathcal{Y}}) = \frac{TP(\mathcal{Y}, \widehat{\mathcal{Y}})}{TP(\mathcal{Y}, \widehat{\mathcal{Y}}) + FN(\mathcal{Y}, \widehat{\mathcal{Y}})} , \quad (19b)$$

$$F1(\mathcal{Y}, \widehat{\mathcal{Y}}) = \frac{Pr(\mathcal{Y}, \widehat{\mathcal{Y}}) Rc(\mathcal{Y}, \widehat{\mathcal{Y}})}{Pr(\mathcal{Y}, \widehat{\mathcal{Y}}) + Rc(\mathcal{Y}, \widehat{\mathcal{Y}})} \quad (19c)$$

In addition to tracking the exact location of the fire front over time, the location of the resulting scar left by the fire is also tracked over time. Predicting the location of the scar is an easier task than predicting the position of the exact fire front, as a correct scar prediction only requires that the model predicted a given scarred cell at some point before the given time point, as opposed to predicting the exact time the cell burnt. All of the same statistics are tracked for the fire scar as for the fire-front itself. We refer to the prediction on the fire front as the ‘burn’ prediction, and refer to the predictions of the fire scar as the ‘ash’ prediction.

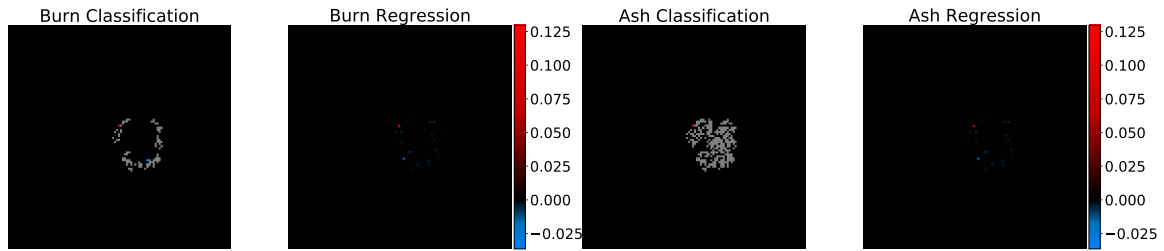
4.2. Example: A Single Prediction

Figure 7 provides an example for a single prediction of a single fire sequence in the *realistic* dataset. The ConvLSTM model is used to make this prediction, but there are similarly behaving examples for all of the models. There are four rows of results, corresponding to predictions at time instances $t = \{11, 14, 29, 49\}$. Notice that the fire front is actually not a single contiguous front, but instead has a complex and disjoint structure.

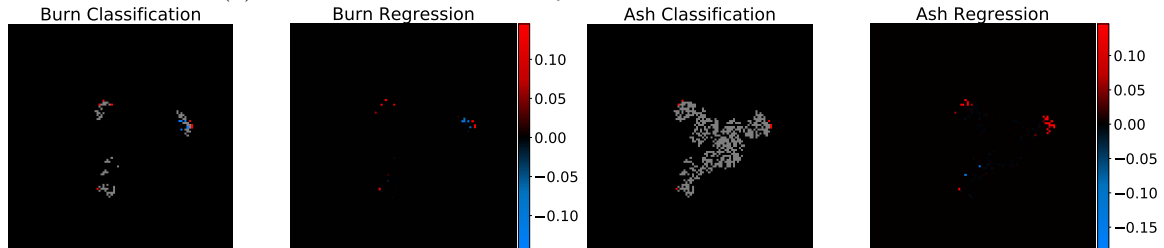
The first prediction for $t = 11$ is nearly perfect, though the *Burn Classification* shows there is a single FP colored in red, indicating that the predicted value was too large, and a single FN colored in blue, indicating that the predicted value was too small. Recall that $t = 11$ is the time of the first prediction since the first ten time steps are included in the first data point. All of the black cells correspond to TNs, and all of the white cells correspond to TPs. The errors indicated in the *Burn Classification* also show up in the *Burn Regression* graph, where the red and blue colors now indicate the magnitude of the error. In this first prediction, the *Ash* predictions are very similar to the *Burn* predictions.

For the fire-spread prediction at $t = 14$, there are now more errors, as is typical, but it is clear that the model provides realistic predictions. For the consecutive prediction at $t = 29$, there is clear evidence that the model has made errors in the speed at which it propagates the fire front. The red cells show where the model predicts the fire location, whereas the blue cells show the actual fire location. Also note in the *ash* results that most of the red cells are still there, but most of the blue cells are missing. This is because those blue cells had burnt away in previous predictions, so the fire scar for those cells is now correct. This highlights why the ash prediction is less punishing to some errors than the burn prediction.

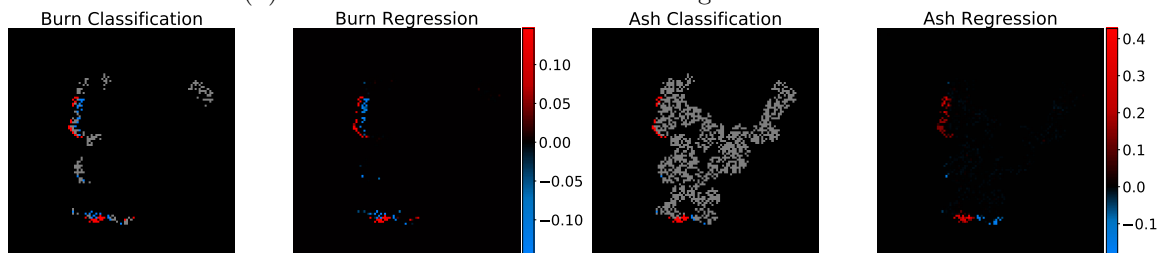
Figure 8 shows statistical results as a function of time for this one single fire sequence. The first two graphs demonstrate that the ConvLSTM adequately predicts the overall size of the fire for the transient fire sequence as well as the overall location of the fire front. The classification stats show that the F1 burn score (Fig. 8(c)) never dropped below 0.8, and that the F1 ash score (Fig. 8(d)) never dropped below 0.95. Notice that both F1 scores drop to the lowest point somewhere between the 25th and 30th consecutive prediction. This is a typical behavior for the *ash* prediction, as most fire sequences in the corpus ultimately burn down most of the forest (and so if the prediction is doing anything reasonable, by the end of the sequence, it will have accurately predicted that most if not all of the vegetation is consumed by the fire). However, this is less typical for the burn classification, as detecting the exact location of the fire front over time is often monotonically decreasing in quality.



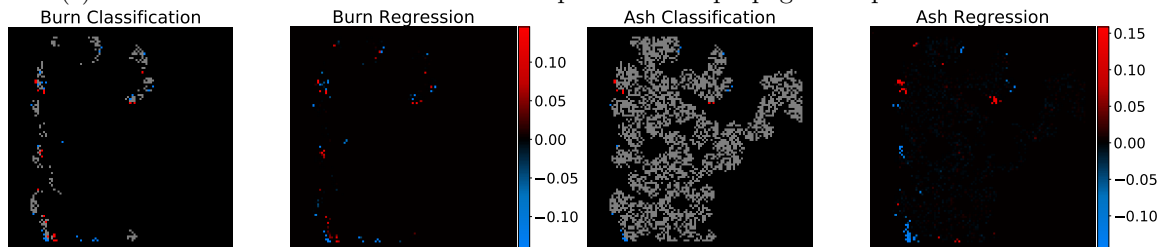
(a) Prediction at $t = 11$: Very few errors at initial instance.



(b) Prediction at $t = 14$: Errors starting to accumulate.



(c) Prediction at $t = 29$: Indication of overprediction of propagation speed of fire front.



(d) Prediction at $t = 49$: Fewer error at final burn-out state of the fire.

Figure 7: Visualization of four predictions from a single predicted fire sequence. *Classification* graphs show the classification errors. Red cells are false positives (FP). Blue cells are false negatives (FN). Black and white cells are properly classified cells. *Regression* graphs show the regression errors. Note that not all regression errors were significant enough to cause classification errors.

4.3. Corpus Results

We proceed by extending the analysis of a single training instance to the entire corpus. This is accomplished by summing the errors, and confusion matrix terms, of each of the training instances generated from a single fire sequence, across all of the fire sequences in the validation corpus. Let \mathcal{T} be the set of all training instances generated from a single fire

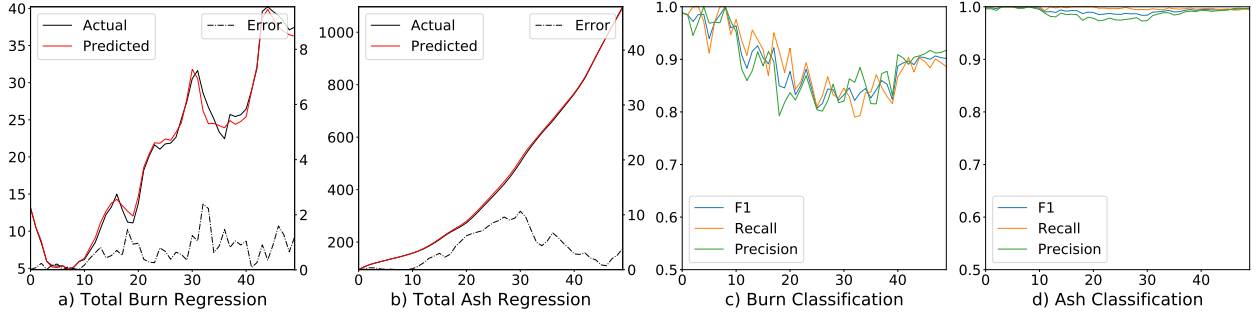


Figure 8: Statistical analysis for the fire sequence over time seen in Fig. 7.

sequence and let \mathcal{Z} be the set of all fire sequences, such that $\forall \mathcal{X}, \mathcal{X} \in \mathcal{T}$ and $\forall \mathcal{T}, \mathcal{T} \in \mathcal{Z}$. Let $\mathcal{Y}_{\mathcal{X}}$ and $\hat{\mathcal{Y}}_{\mathcal{X}}$ be the label and the prediction for the training instance \mathcal{X} . Then, the tracked stats can then be computed via:

$$MSE(\mathcal{Z}) = \frac{1}{d} \sum_{\mathcal{T} \in \mathcal{Z}} \sum_{\mathcal{X} \in \mathcal{T}} MSE(\mathcal{Y}_{\mathcal{X}}, \hat{\mathcal{Y}}_{\mathcal{X}}) \quad (20a)$$

$$STE(\mathcal{Z}) = \frac{1}{d} \sum_{\mathcal{T} \in \mathcal{Z}} \sum_{\mathcal{X} \in \mathcal{T}} STE(\mathcal{Y}_{\mathcal{X}}, \hat{\mathcal{Y}}_{\mathcal{X}}) \quad (20b)$$

$$TP(\mathcal{Z}) = \sum_{\mathcal{T} \in \mathcal{Z}} \sum_{\mathcal{X} \in \mathcal{T}} TPs(\mathcal{Y}_{\mathcal{X}}, \hat{\mathcal{Y}}_{\mathcal{X}}) \quad (20c)$$

where d is the total number of fire sequences in the validation dataset. The remaining confusion matrix terms (FP, TN, FN) are similarly defined and the rates of these terms, and the F1 and Precision metrics, remain unchanged.

4.4. CNN Results

As mentioned in Section 3.2, we investigated an autoencoder-like CNN that includes downsampling stages. We refer to this model as the *CNN-Autoencoder* model. Ultimately, this model did not perform well, and we simplified the structure, which we refer to as the *CNN-Simplified* model. As mentioned in Section 3.5, a lower-bound on the prediction created by the CNN was used to stop the slow accumulation of errors across many consecutive predictions. The model using this threshold is referred to as the *CNN-Thresholded* model.

Figure 9 compares the performance of these three CNN models for the four datasets. Notice that the *CNN-Autoencoder* has the lowest F1 score on all datasets, both on the *burn* and the *Ash* results. However, *CNN-Simplified* has much higher regression errors after about 30 consecutive iterations on the *wind* dataset. This is because by then, *CNN-Simplified* has basically started the entire forest on fire, and significantly overpredicts the fuel burn.

CNN-Simplified did better on the remaining three datasets, performing nearly as well as *CNN-Thresholded* in those cases. Interestingly, there was one way the *CNN-Autoencoder* out-performed the other models. On the *wind-slope* dataset, the *CNN-Autoencoder* had lower MSE compared to the other CNNs. We attribute this to the fact that the model prioritizes getting the overall level of fire to be correct, while sacrificing the fidelity in

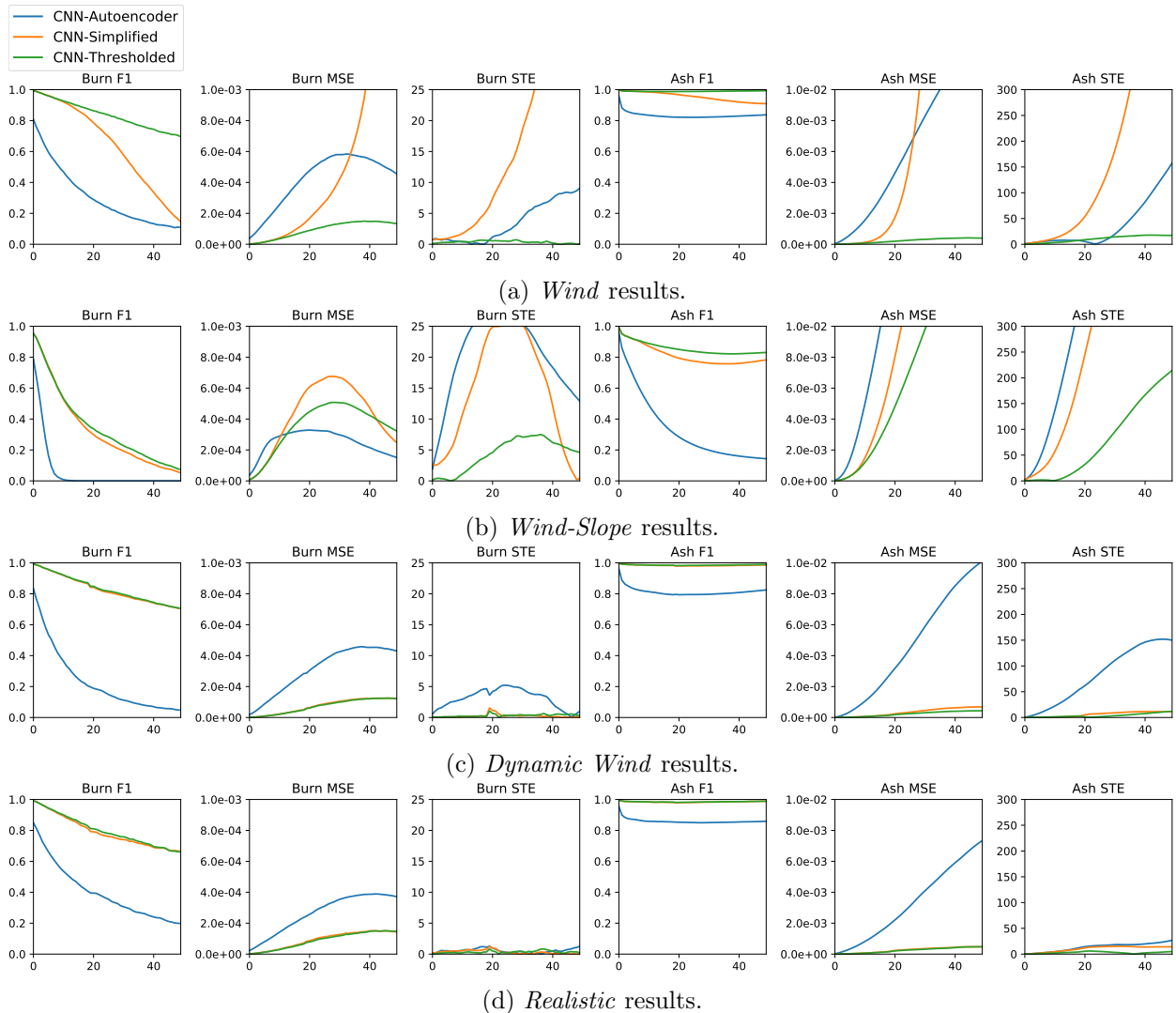


Figure 9: Performance of the CNN models on the four datasets. The horizontal axis on all graphs corresponds to the 50 total consecutive predictions.

accurately predicting the fire location. The *wind-slope* dataset actually ended up being the most challenging dataset for all models. Notice that the *burn* F1 scores for all models on this dataset drop below 0.2 on this dataset, but for the stronger CNN models, the F1 score stays much higher on the other datasets.

Both the *dynamic wind* and *realistic* datasets have an abrupt change of wind direction at the 20th consecutive time step. All models have worse predictions right at this point, as expected, which in the CNN models is most evidently seen in the Burn Total Error graph.

4.5. ConvLSTM Results

Figure 10 compares the results of the ConvLSTM with the best performing CNN on the four datasets. The LSTM dominated the performance of the CNN on the *wind* dataset and

the *wind-slope* dataset. It still maintained an advantage on the F1 score and MSE on the other two datasets, but the advantage was not as pronounced.

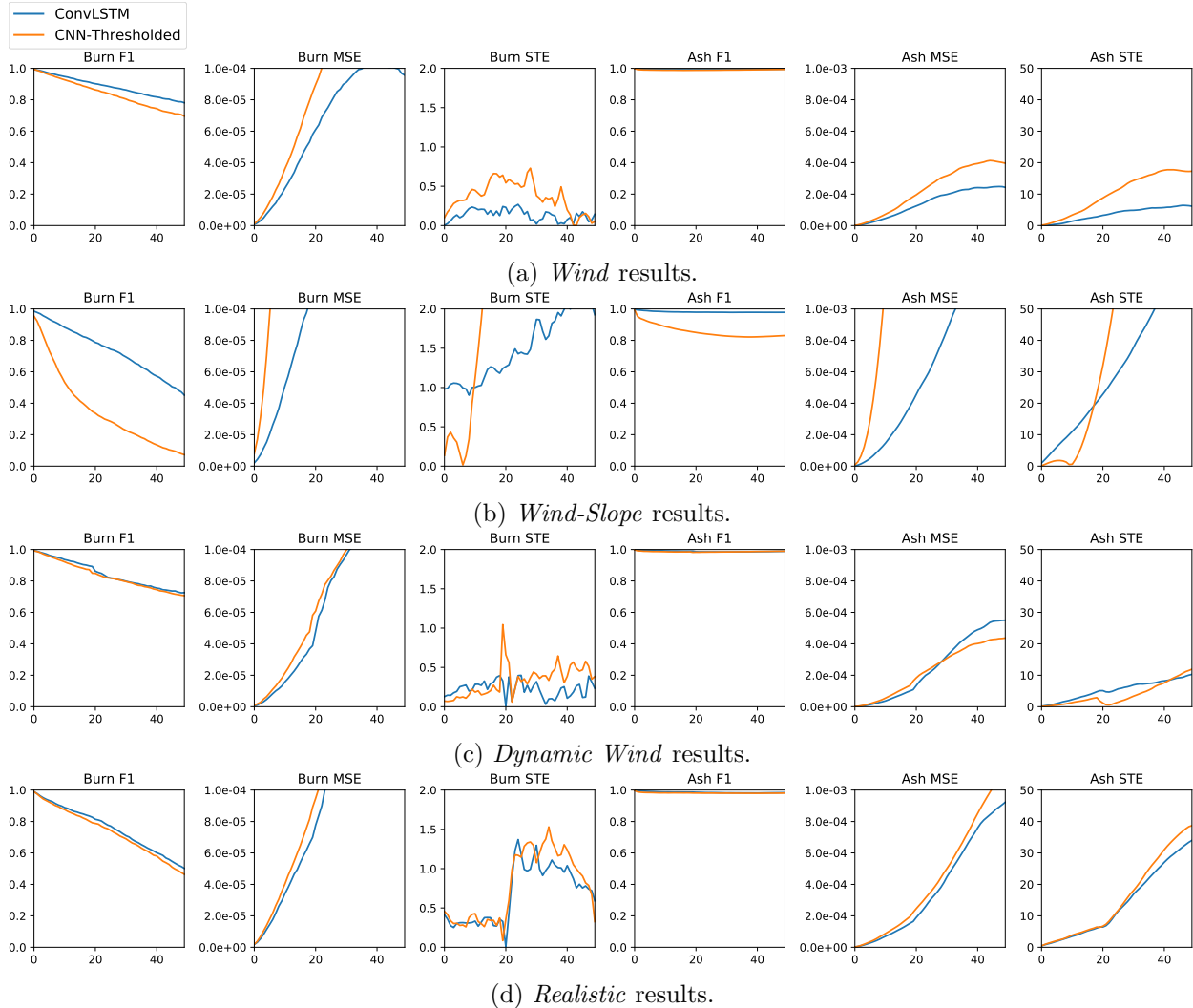


Figure 10: Comparison between the best performing ConvLSTM and the best performing CNN. The horizontal axis on all graphs corresponds to the 50 total consecutive predictions.

Table 3 provides the $F1$, MSE and STE results for several fixed consecutive predictions presented in the graphs. Bolded values indicate that a model’s statistic is better than the corresponding statistic for the other model (i.e., a higher $F1$ score, a lower MSE or a lower STE). In general, the table makes it clear that the ConvLSTM model provides more accurate results than the CNN model, as evident by the better $F1$ and MSE . It typically had the better STE , but the CNN did show some overall strength with the STE , particularly early on in the sequence of predictions. The main exception to the results was in the *Dynamic Wind* dataset after the wind change directions. Recall that the wind changes directions at time step 30 in a fire sequence, which shows up at the 19th consecutive prediction in these

Table 3: Quantitative comparison of modeling results for all datasets on the best performing ConvLSTM and CNN models. Bolded values indicate the model’s statistic is at least as good, or better, than the other model’s corresponding statistic.

	<i>ConvLSTM</i>						<i>CNN-Threshold</i>					
	<i>Burn</i>			<i>Ash</i>			<i>Burn</i>			<i>Ash</i>		
<i>Iter</i>	<i>F1</i>	<i>MSE</i>	<i>STE</i>	<i>F1</i>	<i>MSE</i>	<i>STE</i>	<i>F1</i>	<i>MSE</i>	<i>STE</i>	<i>F1</i>	<i>MSE</i>	<i>STE</i>
Wind dataset												
0	0.992	8.26e-07	0.01	0.999	8.26e-07	0.01	0.993	1.24e-06	0.10	0.998	1.24e-06	0.10
9	0.951	2.02e-05	0.23	0.994	4.05e-05	1.18	0.933	3.10e-05	0.46	0.988	6.28e-05	2.92
19	0.906	5.79e-05	0.24	0.992	1.17e-04	3.04	0.870	8.47e-05	0.64	0.988	1.84e-04	8.24
29	0.866	8.97e-05	0.07	0.993	1.95e-04	4.83	0.810	1.30e-04	0.56	0.989	3.11e-04	13.95
39	0.820	1.05e-04	0.02	0.994	2.40e-04	5.64	0.748	1.48e-04	0.33	0.991	3.91e-04	17.43
49	0.781	9.55e-05	0.14	0.995	2.43e-04	6.16	0.696	1.34e-04	0.05	0.993	3.96e-04	17.27
Wind-Slope dataset												
0	0.985	2.07e-06	0.98	0.996	2.07e-06	0.98	0.953	8.26e-06	0.14	0.993	8.26e-06	0.14
9	0.893	4.42e-05	1.00	0.983	1.25e-04	10.04	0.570	2.09e-04	0.80	0.893	9.62e-04	0.51
19	0.798	1.12e-04	1.25	0.980	4.18e-04	21.60	0.347	4.35e-04	4.34	0.853	4.38e-03	27.41
29	0.705	1.62e-04	1.69	0.979	8.17e-04	35.95	0.237	5.07e-04	7.25	0.829	9.31e-03	88.69
39	0.582	1.77e-04	2.00	0.979	1.23e-03	54.20	0.143	4.33e-04	6.58	0.822	1.38e-02	160.44
49	0.451	1.63e-04	1.93	0.978	1.62e-03	75.58	0.072	3.22e-04	4.62	0.831	1.59e-02	214.25
Dynamic Wind dataset												
0	0.992	4.13e-07	0.13	0.999	4.13e-07	0.13	0.992	8.26e-07	0.07	0.998	8.26e-07	0.07
9	0.943	1.32e-05	0.21	0.992	3.18e-05	2.00	0.929	1.82e-05	0.23	0.986	4.63e-05	1.14
19	0.892	3.88e-05	0.33	0.990	1.08e-04	5.08	0.849	5.83e-05	1.04	0.982	1.63e-04	1.85
29	0.803	9.34e-05	0.27	0.985	3.03e-04	6.58	0.800	9.67e-05	0.44	0.985	2.96e-04	2.96
39	0.760	1.16e-04	0.26	0.986	4.80e-04	8.12	0.749	1.21e-04	0.30	0.987	3.99e-04	7.18
49	0.725	1.14e-04	0.23	0.989	5.50e-04	10.28	0.706	1.22e-04	0.39	0.990	4.36e-04	11.90
Realistic dataset												
0	0.989	1.65e-06	0.41	0.998	1.65e-06	0.41	0.989	2.07e-06	0.46	0.996	2.07e-06	0.46
9	0.898	2.98e-05	0.32	0.988	6.07e-05	3.16	0.883	3.60e-05	0.42	0.982	7.69e-05	3.43
19	0.827	6.98e-05	0.33	0.987	1.64e-04	6.43	0.792	8.93e-05	0.09	0.981	2.22e-04	6.36
29	0.721	1.45e-04	1.16	0.982	4.12e-04	15.63	0.699	1.60e-04	1.29	0.980	4.73e-04	17.04
39	0.612	2.14e-04	0.95	0.982	7.26e-04	25.98	0.585	2.31e-04	1.30	0.979	8.14e-04	29.80
49	0.502	2.45e-04	0.59	0.984	9.22e-04	33.98	0.464	2.61e-04	0.33	0.981	1.13e-03	38.69

tables (since the first 10 time steps are used to generate the first prediction, and the initial prediction is zero-indexed). The *Burn* results weren’t actually better for the CNN in this range though. One possible explanation is that at the time the wind changed directions, the ConvLSTM model made some errors that caused a momentary error in the *Burn* results, which left behind permanent errors in the accumulating *Ash* results. Those errors can permanently damage the *Ash* statistics without permanently damaging the *Burn* statistics since once the fire front moves away from the errors, the correct fire front can still exist.

Overall, the results confirm that the ConvLSTM does a significantly better job predicting the exact location of the fire, and to a smaller degree, the overall amount of fire, than the CNN. Interestingly, in the earlier predictions, the CNN model sometimes had better *STE*, which would then get worse in later predictions. This is likely due to the CNN prioritizing making overall amounts of fire predictions correctly, but then errors in identifying exactly which cells were on fire ultimately lead to an errant fire propagation that made subsequent accurate estimations of total burn impossible.

4.6. Unexpected Results

One of the most surprising results was the fact that the *wind-slope* dataset was the hardest dataset to classify. This was the dataset that likely had the least coverage in the training corpus in terms of interacting forces on the fire front. Each corpus has exactly 800 fire sequences for training and 200 fire sequences for testing. Each sequence has a constant randomized wind, and a constant randomized planar slope. Thus, in the *wind* dataset, there are approximately two training samples for each of the 360 possible degrees of wind direction, meaning that most validation samples likely had a training sample with a similar wind direction. However, with the *wind-slope* dataset, the joint space of wind direction and slope direction has far less coverage, so a validation example with a given wind and terrain slope likely has no exact counterparts in the training data. Both the *dynamic-wind* and *realistic* datasets don't suffer from this issue as much since their slopes are not planar. The more realistic elevation maps they use will have good coverage in the training data, and also likely constrains the direction a fire could propagate (thus making classification easier). This is particularly true on the *realistic* dataset where the elevation and the patterns of vegetation do not necessarily align realistically in the underlying percolation model, further constraining where the fire can spread (and further making classification easier).

The ConvLSTM model outperformed the CNN model most significantly on *wind-slope*. This suggests that as the difficulty of the underlying prediction increases, the benefit the ConvLSTM brings grows. We hypothesize that the ConvLSTM acts as a type of error correction, in which errant predictions at one consecutive prediction are ignored in subsequent consecutive predictions by the memory cells of the LSTM. However, one main drawback in using DNNs in general is that identifying the reason a DNN makes its predictions is difficult. Indeed, interpreting a learned DNN model remains an active area of research [30].

Another surprising result was that while the CNN models struggled on the *wind* dataset when compared to the ConvLSTM, it didn't struggle nearly as much on the *dynamic wind* dataset. The *dynamic wind* dataset behaves similarly to the *wind* dataset before the 30th consecutive prediction, so we expected the predictive performance to be similar up until this point. However, there is one main difference between these datasets. The *dynamic wind* dataset has stronger absolute wind levels. This was necessary as we found that using wind values that were of the same general strength of the *wind* dataset resulted in many fires simply burning out after the wind change. Increasing the wind velocity resolved that issue, but had an unintended consequence. The larger winds caused the fires to burn larger fractions, which ultimately makes predictions easier. There is a relationship between how much forest has burnt, and how difficult the underlying predictions are, and the exact nature of that relationship remains an open question.

5. Conclusions and Future Work

The primary contribution made in this work is the demonstration that the Convolutional Long Short-Term Memory (ConvLSTM) deep neural network is capable of capturing the transient dynamics of wildland fires. To the best of our knowledge, this work represents one of the first attempts to model such data, along with the previous work of Hodges and

Lattimer [10] and Radke et al. [11]. Previous work focused on making a single prediction for a relatively large time step (hours or days). We instead focus on an autoregressive process, making predictions mere minutes into the future, and consecutively repeating those prediction to extend to larger periods of time.

As sufficiently detailed empirical wildland fire data does not currently exist, we demonstrate the efficacy of the ConvLSTM model on several corpuses of simulated data generated by a semi-empirical cellular automaton percolation model. Four distinct data corpuses were tested, each with an increasing amount of complexity. The first corpus was the simplest, only including a single source of constant wind as a possible confounding factor. The second corpus adds a planar slope to the terrain as an additional factor. The third corpus introduces an abrupt change in wind direction to test how effectively the models can deal with temporally changing conditions. The final corpus adds varying moisture content to the fuel and creates a more realistic distribution of foliage.

It was initially expected that as the underlying corpus was made more complex, the general classification difficulty would increase. But surprisingly, the most difficult to classify corpus was the second corpus with just wind and a planar slope. We hypothesize that this is due to the limited coverage of the joint space of wind velocity and terrain-slope direction in the training data, which may require the highest level of generalization in the trained models to properly predict the validation data. There also appears to be a relationship between how quickly a fire spreads, and how difficult the fire is to classify. Fires that spread quickly, and burn large areas of vegetation, are easier to classify than fires that burn more slowly, and burn smaller, more selective areas of vegetation. Future work is warranted to identify the exact nature of that relationship.

We compare the performance of the ConvLSTM to another class of widely employed deep neural networks: (non-temporal) Convolutional Neural Networks (CNNs). After performing a hyperparameter search to empirically identify the best-performing ConvLSTM and CNN, we demonstrate that the ConvLSTM provides improved predictions of the fire-front dynamics, as well as better predicting the rate at which the fire spreads.

In general, we found that simpler variants of both the ConvLSTM and the CNNs outperformed more complicated versions. For example, in the ConvLSTM, we found that residual links and batch normalization layers reduced overall performance. For the CNNs, we found that the complex autoencoder-like model (including downsampling and upsampling layers) performed worse than a simpler CNN with just a few stacked convolutional layers.

The results are an encouraging signal for using deep neural networks to model wildland fire propagation, though there is certainly future work that could be considered. First, the complexity of the underlying simulation could be extended with additional physics, or equivalently considering other popular semi-empirical models such as that of Rothermel [2]. Extending to the third dimension would also help, as fire dynamics are inherently a three-dimensional phenomena [31]. Building a model on 3D patches is challenging due to the greatly increased memory requirement, but doing so would allow the ML model to make more accurate predictions.

Second, the predictive performance of the underlying DNN models could likely be improved. Our work demonstrated that relatively simple models are efficacious, but there are a

large number of possible modifications and different approaches that could be investigated, including:

- Replace the least squares loss function with a more sophisticated probabilistic model, potentially by adding TENSORFLOW Probability layers as described in [32].
- Replace convolution operations with attention-based mechanisms, as described in [33, 34, 35].
- Investigate other popular networks, like the CNN-LSTM described in [36, 37], or the UNETs described in [38] and/or the ResNets described in [25].

Acknowledgments

We would like to thank the contributions made to this work by the members of Google’s AI For Weather Team: Jason Hickey, Cenk Gazen, Shreya Agrawal, as well Qing Wang, Yi-Fan Chen, John Anderson, Carla Bromberg, Stephan Hoyer and Casper Sonderby for their guidance which accelerated much of the modeling and experimentation required for this work. Finally, we’d like to thank Martin Mladenov for the many discussions on extending our work, particularly in the context of Tensorflow Probability.

Supplementary Material

The TENSORFLOW source code for the percolation model is available online at <https://github.com/IhmeGroup/Wildfire-TPU> and can be used for generation of data. All data used for training, testing, and validation the ML-models are available through the Kaggle-data repository at <https://www.kaggle.com/johnburge>. Sample codes for the generation of the CNNs and ConvLSTM used in this work are available upon request to the author.

References

- [1] P. Jain, S. C. P. Coogan, S. G. Subramanian, M. Crowley, S. Taylor, and M. D. Flannigan. A review of machine learning applications in wildfire science and management. *Environ. Rev.*, 28(4):478–505, 2020.
- [2] R. C. Rothermel. A mathematical model for predicting fire spread in wildland fuels. Research Paper INT-115, US Department of Agriculture, Intermountain Forest and Range Experiment Station, Ogden, UT 84401, 1972.
- [3] F. A. Albini. Estimating wildfire behavior and effects. General Technical Report INT-30, US Department of Agriculture, Intermountain Forest and Range Experiment Station, Ogden, UT 84401, 1976.
- [4] E. A. Catchpole, N. J. de Mestre, and A. M. Gill. Intensity of fire at its perimeter. *Aust. For. Res.*, 12:47–54, 1982.
- [5] J. A. Del Real. Can data help fight big fires? Firefighters are betting on it. *New York Times*, Jun 24, 2019. <https://www.nytimes.com/2019/06/24/us/wildfires-big-data-california.html>.
- [6] A. L. Sullivan. Wildland surface fire spread modelling, 1990-2007. 1: Physical and quasi-physical models. *Int. J. Wildland Fire*, 18:349–368, 2009.
- [7] A. L. Sullivan. Wildland surface fire spread modelling, 1990-2007. 2: Empirical and quasi-empirical models. *Int. J. Wildland Fire*, 18:369–386, 2009.

- [8] P. Cortez and A. d. J. R. Morais. A data mining approach to predict forest fires using meteorological data. In *Proceedings of the 13th Portuguese Conference on Artificial Intelligence (EPIA)*, pages 512–523, Guimarães, Portugal, 2007.
- [9] V. I. Kozik, E. S. Nezhevenko, and A. S. Feoktistov. Adaptive prediction of forest fire behavior on the basis of recurrent neural networks. *Optoelectronics, Instrumentation and Data Processing*, 49(3):250–259, 2013.
- [10] J. L. Hodges and B. Y. Lattimer. Wildland fire spread modeling using convolutional neural networks. *Fire Technol.*, 55(6):2115–2142, 2019.
- [11] D. Radke, A. Hessler, and D. Ellsworth. FireCast: Leveraging deep learning to predict wildfire spread. In *Proceedings of the Twenty-Eighth International Joint Conference on Artificial Intelligence, IJCAI-19*, pages 4575–4581. International Joint Conferences on Artificial Intelligence Organization, 2019.
- [12] D. E. Rumelhart, G. E. Hinton, and R. J. Williams. Learning representations by back-propagating errors. *Nature*, 323:533–536, 1986.
- [13] X. Shi, Z. Chen, H. Wang, D.-Y. Yeung, W.-k. Wong, and W.-c. Woo. Convolutional LSTM network: A machine learning approach for precipitation nowcasting. In *Proceedings of the 28th International Conference on Neural Information Processing Systems - Volume 1, NIPS’15*, page 802–810, 2015.
- [14] P. V. Arun, K. M. Buddhiraju, and A. Porwal. CNN based sub-pixel mapping for hyperspectral images. *Neurocomputing*, 311:51–64, 2018.
- [15] K. Zhang, X. Geng, and X. Yan. Prediction of 3-d ocean temperature by multilayer convolutional LSTM. *IEEE Geosci. Remote. Sens. Lett.*, 17(8):1303–1307, 2020.
- [16] Z. Zhong, A. Y. Sun, Q. Yang, and Q. Ouyang. A deep learning approach to anomaly detection in geological carbon sequestration sites using pressure measurements. *J. Hydrol.*, 573:885–894, 2019.
- [17] G. Cruz and A. Bernardino. Learning temporal features for detection on maritime airborne video sequences using convolutional LSTM. *IEEE Trans. Geosci. Remote Sens.*, 57(9):6565–6576, 2019.
- [18] D. Ienco, R. Interdonato, R. Gaetano, and D. H. T. Minh. Combining Sentinel-1 and Sentinel-2 satellite image time series for land cover mapping via a multi-source deep learning architecture. *ISPRS J. Photogramm. Remote Sens.*, 158:11–22, 2019.
- [19] T. Beer and I. G. Enting. Fire spread and percolation modelling. *Math. Comput. Model.*, 13(11):77–96, 1990.
- [20] M. Abadi, A. Agarwal, P. Barham, E. Brevdo, Z. Chen, C. Citro, G. S. Corrado, A. Davis, J. Dean, M. Devin, S. Ghemawat, I. Goodfellow, A. Harp, G. Irving, M. Isard, Y., R. Jozefowicz, L. Kaiser, M. Kudlur, J. Levenberg, D. Mané, R. Monga, S. Moore, D. Murray, C. Olah, M. Schuster, J. Shlens, B. Steiner, I. Sutskever, K. Talwar, P. Tucker, V. Vanhoucke, V. Vasudevan, F. Viégas, O. Vinyals, P. Warden, M. Wattenberg, M. Wicke, Y. Yu, and X. Zheng. TensorFlow: Large-scale machine learning on heterogeneous systems, 2015. Software available from <https://www.tensorflow.org>.
- [21] A. Fournier, D. Fussell, and L. Carpenter. Computer rendering of stochastic models. *Commun. ACM*, 25(6):371–384, 1982.
- [22] I. Goodfellow, Y. Bengio, and A. Courville. *Deep Learning*. MIT Press, 2016. <http://www.deeplearningbook.org>.
- [23] M. A. Kramer. Nonlinear principal component analysis using autoassociative neural networks. *AIChE J.*, 37(2):233–243, 1991.
- [24] S. Hochreiter and J. Schmidhuber. Long short-term memory. *Neural Comput.*, 9(8):1735–1780, 1997.
- [25] K. He, X. Zhang, S. Ren, and J. Sun. Deep residual learning for image recognition. In *2016 IEEE Conference on Computer Vision and Pattern Recognition (CVPR)*, pages 770–778, Las Vegas, NV, 2016.
- [26] T. Beucler, M. Pritchard, S. Rasp, J. Ott, P. Baldi, and P. Gentine. Enforcing analytic constraints in neural-networks emulating physical systems. *arXiv preprint*, 1909.00912, 2020.
- [27] F. Chollet et al. Keras. <https://keras.io>, 2015.
- [28] D. P. Kingma and J. Ba. Adam: A method for stochastic optimization. In *3rd International Conference for Learning Representations*, San Diego, CA, USA, 2015.
- [29] K. P. Murphy. *Machine Learning: A Probabilistic Perspective*. The MIT Press, 2012.

- [30] Q. Zhang and S.-C. Zhu. Visual interpretability for deep learning: a survey. *arXiv preprint*, 1802.00614, 2018.
- [31] J. Coen. Some requirements for simulating wildland fire behavior using insight from coupled weather–wildland fire models. *Fire*, 1(6):1–18, 2018.
- [32] J. V. Dillon, I. Langmore, D. Tran, E. Brevdo, S. Vasudevan, D. Moore, B. Patton, A. Alemi, M. D. Hoffman, and R. A. Saurous. Tensorflow distributions. *arXiv preprint*, 1711.10604, 2017.
- [33] A. Vaswani, N. Shazeer, N. Parmar, J. Uszkoreit, L. Jones, A. N. Gomez, L. Kaiser, and I. Polosukhin. Attention is all you need. In *31st Conference on Neural Information Processing Systems (NIPS 2017)*, Long Beach, CA, USA, 2017.
- [34] P. Ramachandran, N. Parmar, A. Vaswani, I. Bello, A. Levskaya, and J. Shlens. Stand-alone self-attention in vision models. In *33rd Conference on Neural Information Processing Systems (NeurIPS 2019)*, Vancouver, Canada, 2019.
- [35] J.-B. Cordonnier, A. Loukas, and M. Jaggi. On the relationship between self-attention and convolutional layers. In *8th International Conference for Learning Representations*, 2020.
- [36] J. Donahue, L. A. Hendricks, M. Rohrbach, S. Venugopalan, S. Guadarrama, K. Saenko, and T. Darrell. Long-term recurrent convolutional networks for visual recognition and description. *IEEE Trans. Pattern Anal. Mach. Intell.*, 39(4):677–691, 2017.
- [37] C. K. Sønderby, L. Espeholt, J. Heek, M. Dehghani, A. Oliver, T. Salimans, S. Agrawal, J. Hickey, and N. Kalchbrenner. MetNet: A neural weather model for precipitation forecasting. *arXiv preprint*, 2003.12140, 2020.
- [38] O. Ronneberger, P. Fischer, and T. Brox. U-Net: Convolutional networks for biomedical image segmentation. In N. Navab, J. Hornegger, W. M. Wells, and A. F. Frangi, editors, *Medical Image Computing and Computer-Assisted Intervention – MICCAI 2015*, pages 234–241, Munich, Germany, 2015.